Concept for a Single-Shot Mid-infrared Spectrometer using Synchrotron Radiation

U. Schade[1], E. Ritter[2], P. Hegemann[2], E. F. Aziz[3, 4], K. P. Hofmann[6]

[1]Helmholtz-Zentrum Berlin für Materialien und Energie GmbH, BESSY II, 12489 Berlin, Germany, Ulrich.Schade@Helmholtz-Berlin.de

[2]Humboldt-Universität zu Berlin, Experimentelle Biophysik, 10115 Berlin, Germany

[3]Freie Universität Berlin, Fachbereich Physik, 14195 Berlin, Germany

[4]Helmholtz-Zentrum Berlin für Materialien und Energie GmbH, Abteilung Funktionale Materialien in Lösungen, 12489 Berlin, Germany,

[6]Charité - Universitätsmedizin Berlin , Institut für medizinische Physik und Biophysik, 10117 Berlin, Germany

13.03.2014

Abstract

Several attempts have been made to extend time-resolved mid infrared spectroscopy to higher time resolution. Such methods are either limited to specific samples that are cyclic and therefore allow the reaction under investigation to be repeated multiple times in the same manner, or they lack spectral resolution or sufficient signal-to noise ratio. Here, we report on a single-shot spectrometer concept which overcomes the aforementioned limitations utilizing fast linear detector arrays and highly brilliant infrared synchrotron radiation. The spectrometer may find applications, beside others, for the investigation of irreversible cascades of structural alterations in proteins.

1. Introduction

Mid-infrared (MIR) spectroscopy is a widely used tool to obtain molecular and structural information on matter. Over the years several methods have been developed to follow transient states in dynamic systems in this spectral range, thereby providing insights into the transient interplay of functional groups and/or chemical species. Recently, fs-laser-based broad-band techniques [1,2] were introduced for MIR time-resolved spectroscopy. While most laser-based methods lack spectral bandwidth and/or resolution when compared to interferometric Fourier transform infrared (FT-IR) technique, the latter offers a broader spectral range to observe multiple vibrational frequencies at once. FT-IR spectroscopy does not require the operation of advanced laser technology and became standard technique in most laboratories.

Time-resolved FT-IR spectroscopy includes step-scan [3] and rapid-scan [4] techniques which are now standard options of commercial FT-IR spectrometers. For the step-scan method the movable mirror of the interferometer moves stepwise over the path length according to the desired bandwidth and spectral resolution. At each stop the process under investigation is triggered and the transient of the detector signal is taken. This builds up a data cube of mirror position, detector signal and time, from which the spectra along the transient time axis are calculated. The obtainable time-resolution is limited by the broad-band infrared detector and is for HgCdTe (MCT) detectors in the order of nanoseconds (see for recent work [5]).

Both the techniques with advanced time-resolution, the step-scan technique and the above mentioned laser-based methods, require that the phenomena under investigation are accurately and multifold repeatable. The sample has thus to be stable over thousands of repetitions of the triggering event to ensure a sufficient signal-to-noise ratio (SNR) to follow small structural changes especially in large biomolecules, which are often below 10^{-3} absorbance units as recent work demonstrates (see, for example [6]). Noteworthy, many systems of interest in life science involve processes which are either non-repeatable at all or involve processes whose return kinetics into the initial state is slow and therefore renders step-scan experiments impractical.

The limitations to cyclic systems do not apply to rapid-scan FT-IR spectroscopy. Here, the movable mirror moves fast and the time-revolution is given by the time the mirror needs to complete one scan. A serious drawback of this method is the moderate time-resolution in the order of some milliseconds due to the mechanical constraints of the movable part. Extending this limit into the microsecond time-range is in principle possible, i.e., by stroboscopic techniques, but either again requires cyclic reactions or lacks SNR ratio [7].

Our day's mid-infrared thermal and photon array detectors initially developed for military purposes are on the way to find their place in civil applications in the same way as Si-based charged coupled device (CCD) arrays did decades ago [8]. Multi-pixel detection together with a high spectral detectivity makes such infrared focal plane arrays (FPA) very attractive to scientific spectroscopic applications, e.g., in space research [9], or imaging and microscopic spectroscopy [10]. The acquisition of MIR spectra with 100-microsecond temporal resolution from non-cycling systems could be demonstrated using a dispersive spectrometer equipped with an FPA operating in a so-called rolling mode [11].

This paper reports on a concept for a spectrometer working in the spectral range between 2000 cm^{-1} and 950 cm^{-1} with a desired spectral resolution of 4 cm^{-1}. It is applicable for single-shot spectroscopy with a temporal resolution in the microsecond time range. The spectrometer is especially suited to monitor non-cyclic processes or cyclic processes with slower recovery kinetics. Some scientific applications in molecular chemistry and biophysics are discussed.

The concept is based on a Féry prism [12] spectrograph combined with a linear detector array. Previous dispersive spectrometer approaches utilize blackbody radiator (Globar) as radiation source. Here, the irradiance of the spectrometer entrance slit becomes rather low due to the large throughput (source area x acceptance angle) of the Globar limiting the achievable SNR. The reported concept overcomes this limitation by utilizing infrared synchrotron radiation which is diffraction-limited focused onto the entrance of the spectrometer.

2. Scientific cases

In molecular chemistry a MIR single-shot spectrometer with a high temporal resolution would be key success to understand the nature of the building block of metal-porphyrine based materials in the multidimensional polymeric array [13]. Their dynamic optical, electronic and photophysical properties have created extensive interest in the supramolecular chemistry. Such materials become substantial, for example, in biomimetics and for sensor and drug development [14]. The important role of metal-porphyrine is based on electron and energy transfer in a wider timescale from picoseconds to milliseconds. The proposed spectrometer can take the slower microsecond-dynamics of the building block and expose its correlation with the rest of the polymeric array during its function.

In biophysics and biochemistry MIR spectroscopy is commonly used to gain insight into the molecular alterations of proteins that accompany and facilitate their biological function. It allows monitoring protein secondary structural alterations as well as intramolecular proton transfer processes, interaction of amino acids and the reorganization of water molecules and hydrogen-bonded networks.

In biological systems, a huge number of signal transduction processes (ie. seeing, smelling, hormone reception) are initiated by proteins belonging to the class of G-protein coupled receptors. One of these receptor proteins, whose function is to recieve a chemical, physical or biological signal and transmit it to a G-protein, is rhodopsin which stands at the beginning of vision in the eyes of vertebrates [15].

< Figure 1 >

Light-induced structural changes in rhodopsin on its way from its inactive dark state to the final active state metarhodopsin II is schematically shown in Figure 1. Light absorption causes *cis/trans* isomerization of the prosthetic group and chromophore, the vitamin A derivative 11-*cis*-retinal [16] into all-*trans*-retinal. The thereby induced strain triggers further stepwise conformational changes of the receptor as shown in Figure 1. The early intermediates bathorhodopsin and lumirhodopsin occur on a very fast timescale (picoseconds to nanoseconds)

and do not show large conformational changes of the apoprotein. However, in these intermediates the transfer of the light energy from the chromophore to the protein is already prepared. Within microseconds, metarhodopsin I is then formed by slight movements of the helices. While this intermediate is still inactive, crucial functional parts of the protein are pre-adjusted; thereby preparing the transition to the active state metarhodopsin II, the species that interacts with and activates the next element of the signal transduction cascade, the G protein. This activation step occurs on a timescale from microseconds to milliseconds and is of utmost scientific interest. Rearrangements that occur upon formation of metarhodopsin II include helix movements, loop movements and a helix elongation. An overview on the infrared spectra of the rhodopsin cascade up to this state is given in Ref. [6], detailed spectra of sub-states of metarhodopsin II are shown in Ref. [17]. Metarhodopsin II is however not stable but decays irreversibly on a timescale from seconds to minutes by hydrolysis of the retinal Schiff base into the opsin apoprotein and free all-*trans* retinal. In the cell, fresh 11-*cis* retinal is then provided by a complex metabolic process, the retinoid cycle.

To follow the conversion of metarhodopsin I to metarhodopsin II is challenging, since the timescale of microseconds to milliseconds is too fast to be resolved by the rapid-scan technique but the irreversibility of the pathway renders step-scan measurements very difficult. This process will become spectroscopically accessible by the proposed spectrometer.

Recently, channelrhodopsin has experienced heightened interest due to its possible applications in neurophysiology and medicine and made possible the new field of optogenetics [18]. Channelrhodopsin, which is a microbial rhodopsin, serves as a direct light gated ion channel [19]. Here, light absorption through retinal *trans/cis* isomerization switches the molecule from a non-conducting dark state to the conducting state that permits the transfer of cations. When in the dark again, the protein returns to a non-conducting state within milliseconds. Key molecular changes within this photo cycle were studied applying infrared spectroscopy [20]. It requires minutes for the protein to return to the fully dark adapted state even though the conducting state disappears within milliseconds. This behavior is a challenge for the advanced step-scan technique, since the long recovery period of the molecule would require several weeks for a complete measurement, and therefore calls for a single-shot instrument.

3. Spectrometer concept

3.1. Design goals

The aforementioned scientific challenges set the stage for the operating parameters of the spectrometer. To investigate crucial intramolecular changes that accompany formation of the functional states a time-resolution of microseconds is desirable. The spectral range between 2000 and 950 cm^{-1} is of specific interest, since we can observe changes of carbonyl vibrations and protein associated lipids (1800 - 1700 cm^{-1}), changes of secondary structure (amide-I, amide-II), and alterations of the chromophores (1400 - 1200 cm^{-1}). Most of the bands under investigation are relatively broad and a spectral resolution of 4 - 8 cm^{-1} seems to be sufficient. Important is the SNR ratio since conformational changes are often small in comparison to the overall structure producing changes of less than 10^{-3} absorbance units.

3.2. Signal-to-Noise and time-resolution

To estimate the spectrometer performance a circular spectrometer entrance is assumed which is imaged at the exit plane forming a line spectrum. The entrance slit is optimally illuminated by a diffraction-limited radiation source, e.g., synchrotron radiation, and the throughput of the spectrometer matches the illumination optics.

The line spectrum is collected by a linear array of photovoltaic detectors, where the geometrical dimension of one detector pixel along the spectrum defines the exit slit and with it the spectral resolution. The array detector is operating in snap-shot mode and all detector pixels of the linear FPA are detecting simultaneously. This makes the spectrometer insensitive to flux fluctuation for instance caused by mechanical vibrations. The photons hitting the detector pixel are converted into electrons with an efficiency, η. The electrons are accumulated over the integration time, τ_{int}.

< Table 1 >

< Table 2 >

For such a spectrometer system the SNR can be calculated from the read-out noise, n_{RN} , of the read-out integrated circuit (ROIC) and the different signal contributions picked up by the detector pixel and which follow Poisson statistics. The SNR is than given by [21]:

$$SNR = \frac{\tau_{\text{int}}\,\eta\,\Phi_{\Delta\nu}}{\sqrt{\tau_{\text{int}}(\eta\,\Phi_{\Delta\nu} + \eta\,\Phi_{BG} + I_{dark})} + n_{RN}},$$

with $\Phi_{\Delta\nu}$ - the spectral radian flux onto the detector pixel to be measured, Φ_{BG} - the radiant flux from the background falling into the field of view of the detector and for the spectral band the detector is sensitive, and I_{dark} - the dark current of the detector.

Model parameters for the FPA used for the further evaluation are presented in Table 1. The dark current of a pixel is estimated from the "Rule 07" [22] for the given parameters. Rule 07 is an empirical relationship based on the state-of-the-art performance of MCT detectors and MCT FPAs of different makers and is valid for a broad range of cut off wavelengths and temperatures. The data for the radiation source are derived for the infrared beamline IRIS [23] at the electron storage ring BESSY II operating at 1.7 GeV with an electron current stored of 300 mA. The IRIS beamline utilizes synchrotron radiation from a bending magnet. The spectral flux delivered is calculated using the SRW [24,25] code and takes into account flux losses due to the split frontend mirror of the beamline. The source area at the source point inside the dipole magnet is calculated using the formula provided by Hirschmuggl [26]. Table 2 displays the source parameters used to estimate the performance of the spectrometer.

< Figure 2 >

Figure 2 shows the relation between the total numbers of accumulated electrons and the integration time for an MCT detector pixel with two different background temperatures, that is the temperature of the spectrometer optics and the spectrometer housing. The numbers of the accumulated electrons are calculated over the bandwidth of 4 cm^{-1} for a frequency of 950 cm^{-1}. The difference between 77 K and room temperature (RT = 300 K) is not that big showing that

even a relatively small F-number of the cold stop could sufficiently limit unwanted background radiation. This suggests operating the spectrometer at RT with much less technical constraints than cryo-optics would imply for an operation at 77 K. Due to the higher background flux hitting the detector pixel at RT the well capacity is already filled after 70 µs of integration whereas this happens at > 100 µs in case of a 77-K spectrometer. The expected SNR for both the spectrometer temperatures are shown in Figure 3. At 1-µs integration time, the SNR yields 450 for the RT model and 530 for the 77-K model, and at 10-µs we expect 1640 and 2040, for RT and 77 K, respectively. There is no drastic difference in the total flux between the two curves. For integration times shorter than 1 µs, the difference almost vanishes. In this time-regime the system becomes photon noise limited denoting that the contributing noise is only the shot noise from the source. To further increase the SNR for integration times shorter than 1 µs more brilliant infrared sources than a synchrotron are requested. Those sources for the next generation of performance may be found in near future in quasi-broadband quantum cascade lasers [27,28] or by laser-based difference frequency generation (DFG) techniques [29].

< Figure 3 >

A crucial component for a high temporal resolution is the internal ROIC of the linear FPA which serves as an interface between the detector pixels and the post-processing electronics. The achievable frame rate and in turn the spectra rate defines the possible temporal resolution of the system. Especially two-dimensional arrays operating in snap-shot mode have an insufficient low frame-rate integration-time duty cycle. However, the duty cycle could be improved to 100 % reading out the array in rolling mode for temporal resolved spectroscopy [11]. Further improvement is possible with significant higher frame rates in the range of tens of kilohertz using dedicated linear arrays. Together with a parallel read-out handling of the ROIC temporal resolutions better than 20 µs seem to be practicable with ready available linear FPAs. Further improvement could then be achieved by a customized ROIC design.

3.3. Optics design

Our spectrometer optics is based on a Féry prism [12] which not only disperses a beam into a spectrum but also focuses the beam. Generally, prism-based spectrographs have the advantage

of a higher optical transmission when compared to grating spectrographs. They are deployed when spectral width rather than spectral resolution is demanded [30]. In addition, they do not suffer from order effects and stray light. The spectrometer proposed here basically follows the optical design of Warren et al. [31], which is based on aplanatic conditions and was derived from earlier designs of Wilson [32]. The advantage of this design is an almost coma and aberration free image together with a flat image plane suitable for modern FPA detectors. The core spectrometer consists of a Féry prism and a spherical mirror. The two spherical surfaces of the prism operate close to their aplanatic conjugates while the spherical mirror close to its center of curvature. The prism is made of BaF_2 which ensures a fast f/number of the spectrometer due to its low index of refraction [31].

< Figure 4 >

A schematic of the spectrometer is shown in Figure 4. The entrance arm and exit arm of the spectrometer core are spatially separated by a block of two plane mirrors which fold the beam for both the optical arms by approximately 90°. This provides enough space for the entrance and detector optics, respectively. The latter consist of a re-imaging system made of two Ge lenses. The lenses are anti-reflection coated in order to minimize reflection losses in the spectral working range. The re-imager has a 1:1 magnification and is designed to fit the F/number of 1.5 of the detector's cold shield.

< Table 3 >

A preliminary solution for the optical design of the spectrometer was found following the recipe of Warren et al. [31] that was consequently optimized by performing non-sequential ray tracing computations with both the software packages SYNOPSIS [33] and Zemax [34]. The optimized parameters for the optical elements of the spectrometer core are summarized in Table 3.

< Figure 5 >

Figure 5 shows the ray aberrations in the focal plane of the spectrometer for the wavelength region of about 8 µm for five different wavelengths 25 nm apart from each other. This distance corresponds to a spectral resolution of approximately 4 cm^{-1}. The size of the ray aberration is

less than 15 µm in diameter and with it much smaller than the point spread function indicated in Figure 5 by the airy disk confirming a diffraction limited operation at this wavelength. This behavior of the design can be maintained over the entire desired spectral range.

< Figure 6 >

The resolving power of the spectrometer was estimated using the Rayleigh criterion, assuming that two spectral spots can be resolved at the focal plane when they are spatially separated by the radius of the airy disk. The resolving power is shown in Figure 6 as a function of wavelength and is compared with a calculated resolving power necessary to obtain an exemplary spectral resolution of 4 cm^{-1}. The intersection between the two lines demonstrates that this resolution can be achieved for wavenumbers lower than 1600 cm^{-1} and even gets higher with further decreasing wavenumbers. However, above 1600 cm^{-1} the resolution is larger than 4 cm^{-1} and reaches about 6.7 cm^{-1} at 2000 cm^{-1}. While the resolving power describes the theoretical maximum of the resolution defined only by the optics, the actual value depends on the lateral dispersion at the focal plane and the pixel pitch of the detector elements.

< Figure 7 >

Finally, Figure 7 shows the lateral dispersion of the spectrometer at the focal plane which steadily decreases upon decreasing wavenumbers. In addition, the linear dispersion necessary to resolve 4 cm^{-1} is exemplarily displayed in the Figure 7 for linear arrays with two different pixel pitches. While an array with a pixel pitch of 15 µm would meet the lateral dispersion of the spectrometer almost over the entire spectral range, an array with a pixel pitch of 40 µm fulfills the requirement only for wavelengths lower than 1400 cm^{-1} and provides a spectral resolution of about 12 cm^{-1} at 2000 cm^{-1}.

4. Summary

Dispersive MIR spectrometers together with modern focal plane technology can provide a tremendous benefit in terms of signal-to-noise ratio and time-resolution originated in the high brilliance of diffraction limited broadband sources.

We presented a fast Féry-prism based spectrometer concept producing an almost coma and aberration free spectrum onto a flat image plane which is beneficial for modern FPA detectors. Together with infrared synchrotron radiation the spectrometer provides temporal resolution in the µs-time range by retaining a SNR in the order of 10^3.

The proposed MIR spectrometer addresses the specific sample requirements concerning spectral and temporal resolution necessary to study kinetic systems in biophysics and molecular chemistry constituting the function of molecules over a broader spectral range. In particular, it will become possible to investigate, on the timescale of microseconds, molecular non-cyclic alterations or cyclic alterations where long lasting recovery kinetics is involved.

Acknowledgement

We acknowledge support by the European Research Council (ERC) Advanced Grant TUDOR to K.P.H., by the Helmholtz-Zentrum Berlin für Materialien und Energie and by the BMBF Verbundforschung. U.S. acknowledges discussions with P. Dumas, M. Tobin and A. Marcelli.

References:

[1] M.L. Groot, L.J.G.W. van Wilderen, M. Di Donato, Photochem. Photobiol. Sci 6 (2007) 501.

[2] G.M. Greetham, P. Burgos, Q. Cao, I.P. Clark, P.S. Codd, R.C. Farrow, M.W. George, M. Kogimitzis, P. Matousek, A.W. PARKER, M.R. POLLARD, D.A. Robinson, Z.-J. Xin, M. Towrie, Appl. Spectrosc. 64 (2010) 1311.

[3] W. Uhmann, A. Becker, C. Taran, F. Siebert, Appl Spectrosc 45 (1991) 390.

[4] M.S. Braiman, P.L. Ahl, K.J. Rothschild, Proc. Natl. Acad. Sci. U. S. A. 84 (1987) 5221.

[5] S. Wolf, E. Freier, M. Potschies, E. Hofmann, K. Gerwert, Angew. Chem. Int. Ed. Engl. 49 (2010) 6889.

[6] F. Siebert, Isr. J. Chem. 35 (1995) 309.

[7] P.R. Griffiths, B.L. Hirsche, C.J. Manning, Vib. Spectrosc. 19 (1999) 165.

[8] G.E. Smith, Rev. Mod. Phys. 82 (2010) 2307.

[9] a. Coradini, F. Capaccioni, P. Drossart, A. Semery, G. Arnold, U. Schade, Adv. Sp. Res. 24 (1999) 1095.

[10] L.M. Miller, R.J. Smith, Vib. Spectrosc. 38 (2005) 237.

[11] C.M. Snively, C. Pellerin, J.F. Rabolt, D.B. Chase, Anal. Chem. 76 (2004) 1811.

[12] C. Féry, Astrophys. J. 34 (1911) 79.

[13] G.R. Desiraju, Angew. Chem. Int. Ed. Engl. 34 (1995) 2311.

[14] V. Lin, S. DiMagno, M. Therien, Science (80-.). 264 (1994) 1105.

[15] K.P. Hofmann, P. Scheerer, P.W. Hildebrand, H.-W. Choe, J.H. Park, M. Heck, O.P. Ernst, Trends Biochem. Sci. 34 (2009) 540.

[16] R. Hubbard, G. Wald, J. Gen. Physiol. (1952).

[17] M. Elgeti, A.S. Rose, F.J. Bartl, P.W. Hildebrand, K.-P. Hofmann, M. Heck, J. Am. Chem. Soc. 135 (2013) 12305.

[18] P. Hegemann, G. Nagel, EMBO Mol. Med. 5 (2013) 173.

[19] G. Nagel, D. Ollig, M. Fuhrmann, S. Kateriya, A.M. Musti, E. Bamberg, P. Hegemann, Science 296 (2002) 2395.

[20] E. Ritter, K. Stehfest, A. Berndt, P. Hegemann, F.J. Bartl, J. Biol. Chem. 283 (2008) 35033.

[21] A. Marcelli, W. Xu, D. Hampai, L. Malfatti, P. Innocenzi, U. Schade, Z. Wu, Anal. Bioanal. Chem. 397 (2010) 2095.

[22] W.E. Tennant, D. Lee, M. Zandian, E. Piquette, M. Carmody, J. Electron. Mater. 37 (2008) 1406.

[23] W.B. Peatman, U. Schade, Rev. Sci. Instrum. 72 (2001) 1620.

[24] O. Chubar, P. Elleaume, S. Kuznetsov, A.A. Snigirev, Proc. SPIE 4769 (2002) 145.

[25] O. Chubar, A. Fluerasu, L. Berman, K. Kaznatcheev, L. Wiegart, J. Phys Conf. Ser. 425 (2013) 162001.

[26] C.J. Hirschmugl, Ph.D. Thesis, Yale Univ. (1994).

[27] J. Faist, F. Capasso, D. Sivco, C. Sirtori, A.L. Hutchinson, A.Y. Cho, Science (80-.). 264 (1994) 553.

[28] B. Lendl, J. Frank, R. Schindler, A. Muller, M. Beck, J. Faist, Anal. Chem. 72 (2000) 1645.

[29] W. Chen, J. Cousin, E. Poullet, J. Burie, D. Boucher, X. Gao, M.W. Sigrist, F.K. Tittel, C. R. Phys. 8 (2007) 1129.

[30] Z. Keltner, K. Kayima, A. Lanzarotta, Appl. Spectrosc. 61 (2007) 909.

[31] D.W. Warren, J.A. Hackwell, D.J. Gutierrez, Opt. Eng. 36 (1997) 1174.

[32] R.N. Wilson, Optik (Stuttg). 29 (1969) 17.

[33] D.C. Dilworth, Proc. SPIE 0766 (1987) 264.

[34] J.M. Geary, Introduction to Lens Design: With Practical ZEMAX Examples, Willmann-Bell, Richmond, 2002.

Tables:

Table 1: Model parameters of the MCT FPA detector used in this study.

Cut-off	Dark Current Density @ 77 K	Pixel Size	Well Capacity	Read-out Noise	Cold Stop F#	Convertion Efficiency
950 cm^{-1}	5.4 x 10^{17} $e^-/s/m^2$	25 µm	5 x 10^7 e^-	500 e^- rms	1.5	1e^-/photon

Table 2: Source parameters for the IRIS Beamline at the electron storage ring BESSY II.

Natural Opening Angle	Spectral Flux into IRIS	Source Area	Source Throughput
22 mrad	3.6 x 10^{13} photons/s/0.1 %bdw	3.2 mm^2	4.2 x 10^{-9} srm^2

Table 3: Optimized optical data for the spectrometer following the SYNOPSIS convention. The position of the optical surfaces are given in global coordinates.

Surface	Radius (mm)	Thickness (mm)	Material	α-tilt (°)	y-decenter (mm)	z-decenter (mm)
Object	Inf.	130.2	Air			
1	-58.71	27.66	BaF_2	-5.201	0	10.26
2	-84.16	88.49	Air	23.87	0	37.93
3	-266.5	-265.3	Mirror	-6.732	0	126.4
Image	Inf.	0	Air	10.61	-20	-138.1

Captions:

Figure 1:

Light induced cascade of rhodopsin intermediates. Shown are the dark state Rhodopsin (Rho) with 11-*cis*-retinal (red) in its binding pocket (grey), bathorhodopsin (Batho), lumirhodopsin (Lumi), metarhodopsin I (Meta I), metarhodopsin II (Meta II), all with all-*trans*-retinal (orange). The latter intermediates occur on a timescale interacts with the G-protein (Transducin) and decays irreversibly into the apoprotein (Opsin, grey) and free all-*trans* retinal within minutes.

Figure 2:

Total numbers of accumulated electrons as a function of the integration time calculated for the bandwidth of 4 cm^{-1} at a frequency of 950 cm^{-1}. The well capacity of 5 x 10^7 electrons is indicated.

Figure 3:

Calculated signal-to-noise ratios as a function of the integration time of for two different temperatures of the spectrometer optics.

Figure 4:

Schematic of the optical design of the spectrometer.

Figure 5:

Spot diagram of the spectrometer design for the 8 µm wavelength region.

Figure 6:

Resolving power of the spectrometer design discussed in text as a function of wavelength based on the Rayleigh criterion. The blue curves represent the resolving power necessary to resolve 4 cm^{-1} over the entire spectral range.

Figure 7:

Lateral dispersion of the spectrometer design as a function of wavelength compared with the dispersion necessary for two linear arrays with different pixel pitches.

Figure 1

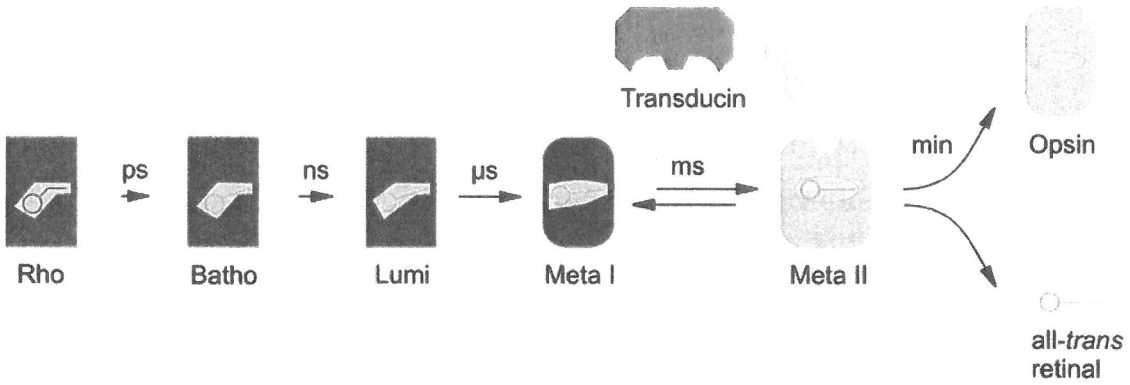

Figure 1

Figure 2

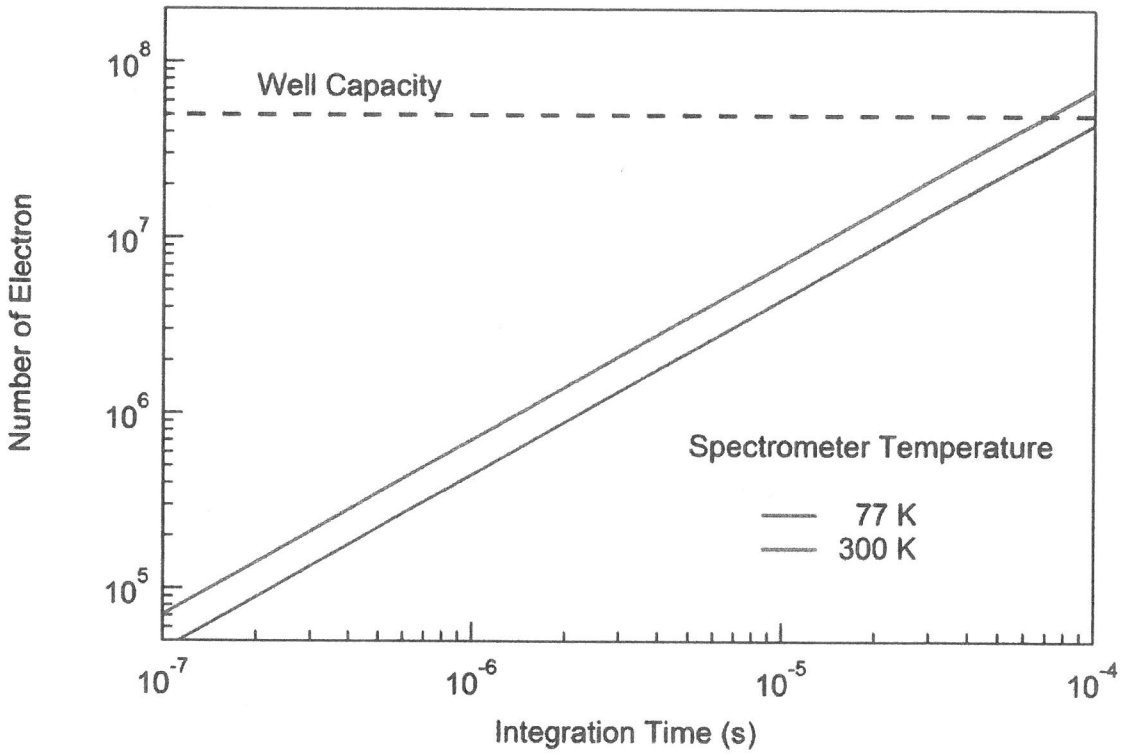

Figure 2

Figure 3

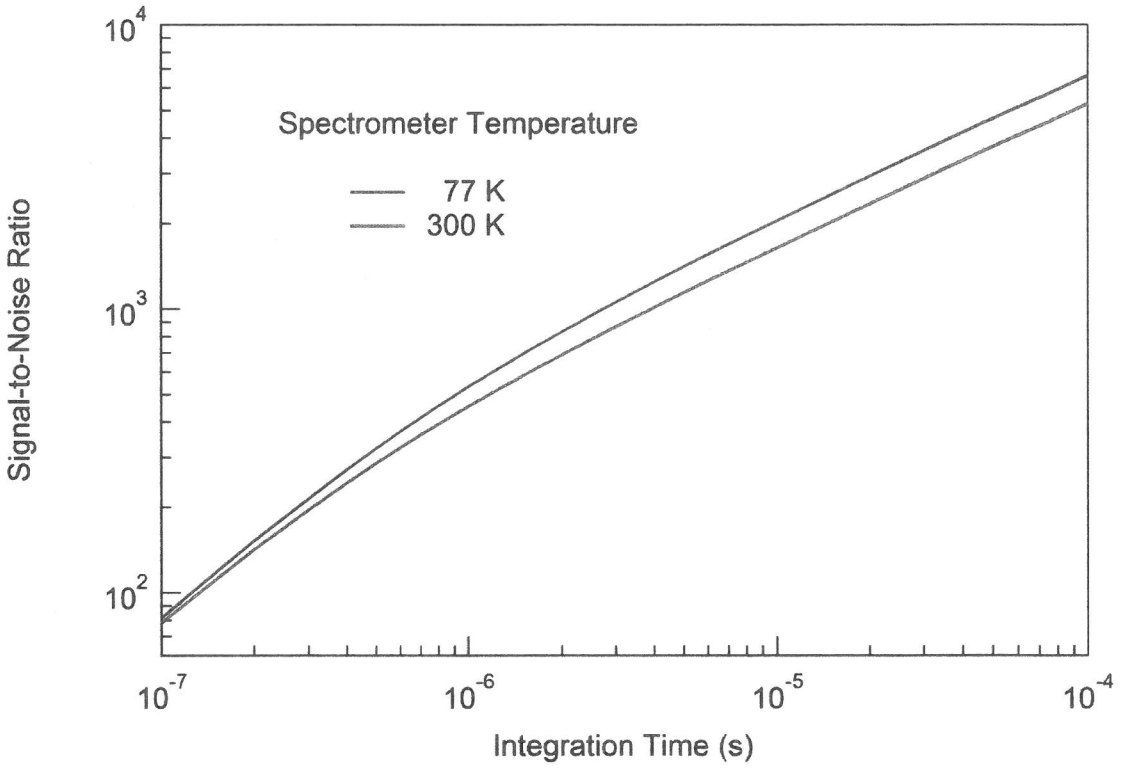

Figure 3

Figure 4

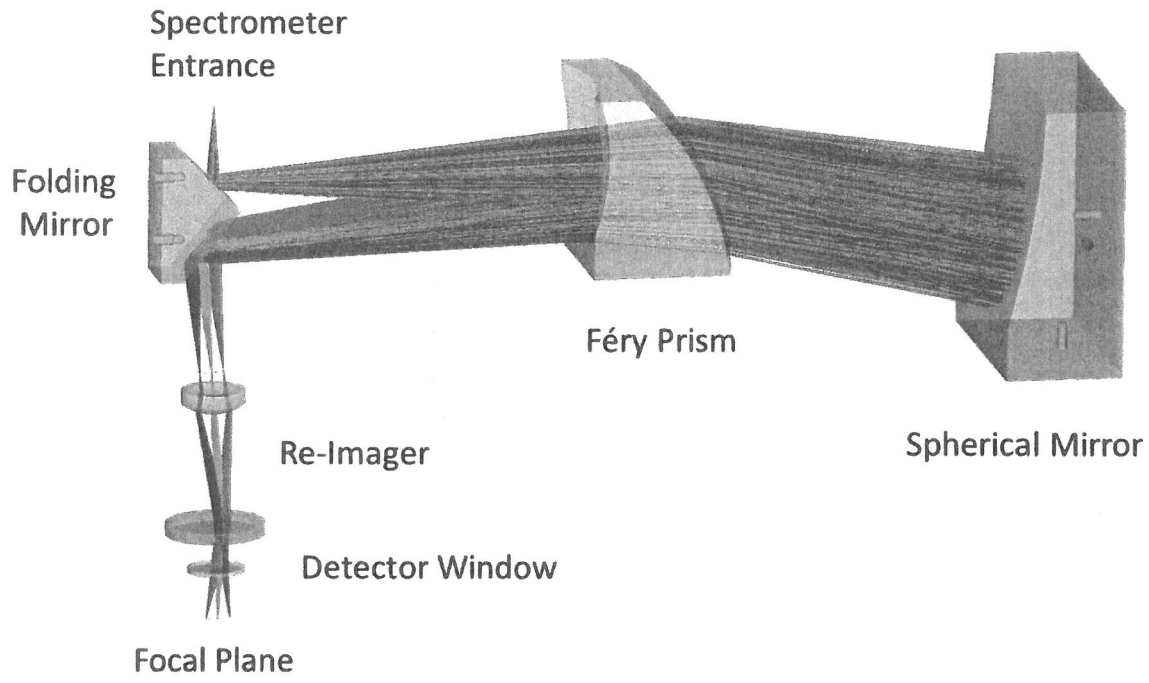

Figure 4

Figure 5

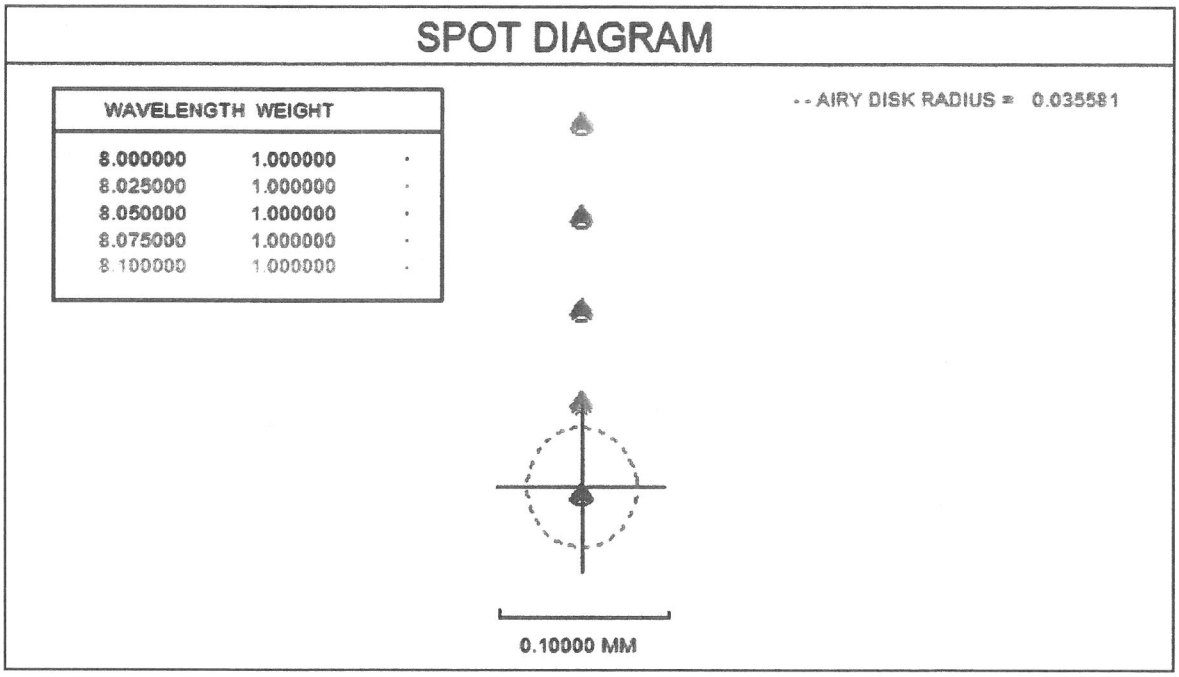

Figure 5

Figure 6

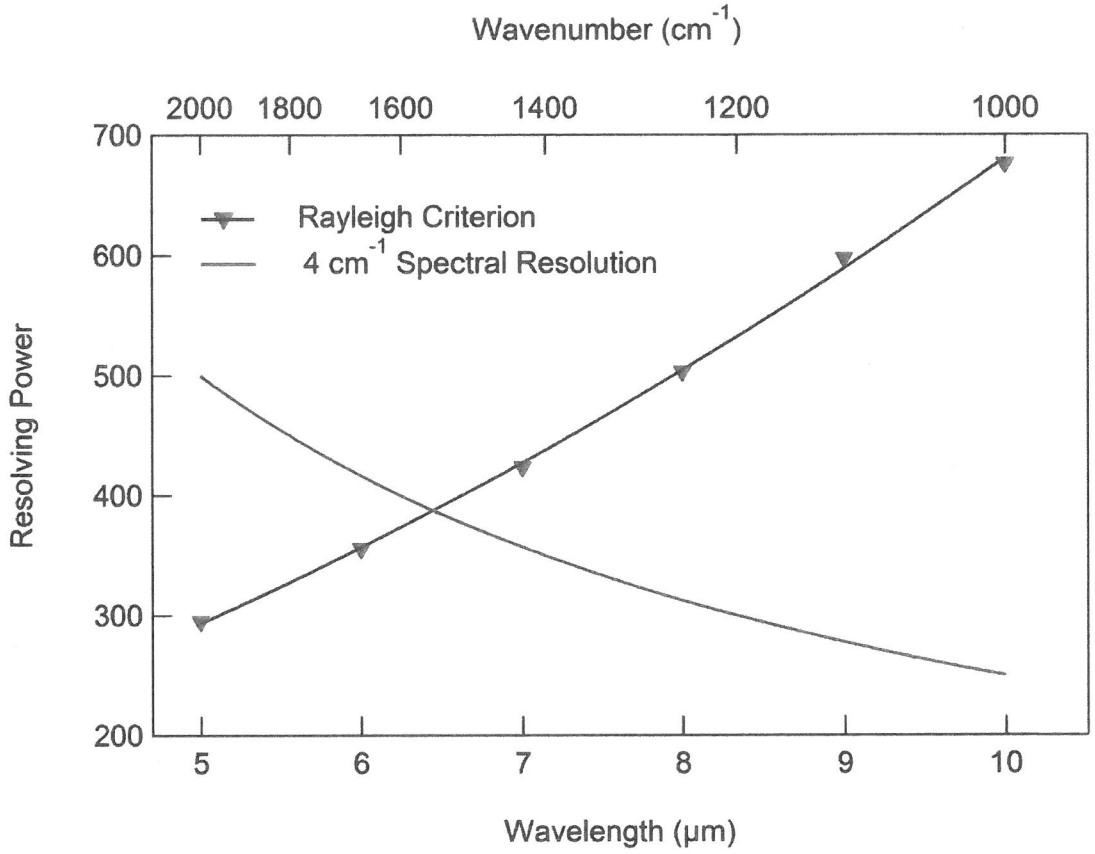

Figure 6

Figure 7

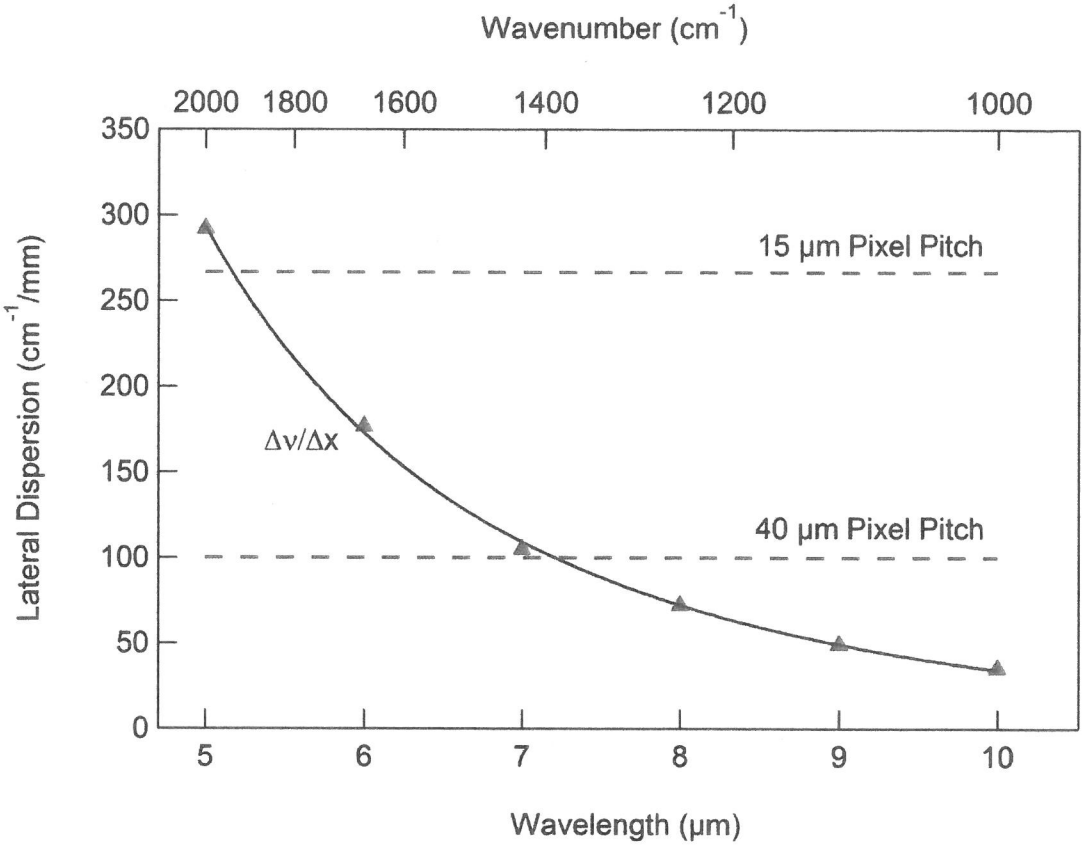

Figure 7